

Kareus: Joint Reduction of Dynamic and Static Energy in Large Model Training

Ruofan Wu

Jae-Won Chung

Mosharaf Chowdhury

University of Michigan

Abstract

The computing demand of AI is growing at an unprecedented rate, but energy supply is not keeping pace. As a result, energy has become an expensive, contended resource that requires explicit management and optimization. Although recent works have made significant progress in large model training optimization, they focus only on a single aspect of energy consumption: dynamic *or* static energy.

We find that fine-grained kernel scheduling and frequency scaling *jointly* and *interdependently* impact both dynamic and static energy consumption. Based on this finding, we design *Kareus*, a training system that pushes the time–energy tradeoff frontier by optimizing both aspects. *Kareus* decomposes the intractable joint optimization problem into local, partition-based subproblems. It then uses a multi-pass multi-objective optimization algorithm to find execution schedules that push the time–energy tradeoff frontier. Compared to the state of the art, *Kareus* reduces training energy by up to 28.3% at the same training time, or reduces training time by up to 27.5% at the same energy consumption.

1 Introduction

Today, energy is the ultimate bottleneck for scaling AI [7, 23, 30]. The energy demand of training large models and serving them to millions is growing at an unprecedented rate [19, 24, 28], with projections indicating that by 2035, nearly 10% of US electricity demand could be from datacenters [23]. However, procuring energy at scale is slow, e.g., three years for natural gas, five to ten years for nuclear [35]. This mismatch makes energy an expensive, contended resource that must be explicitly budgeted, managed, and allocated with efficient systems and optimization methods.

In this context, large model training is a key target for optimization; a single training run can consume enough energy to power more than 24,000 average US households for a month [1, 24]. To understand the current state of large model training optimizations, we analyze them through the lens of *dynamic* (consumed by actual work) and *static* (consumed at all times regardless of work) energy consumption of GPUs (§2). *Perseus* [15] reduces dynamic energy by scaling the frequency of computations off the critical path, but does not reschedule kernels. Recent works in fine-grained kernel scheduling [17, 37, 42] reduce static energy by overlapping computation and communication, but ignore dynamic energy and frequency scaling. Therefore, we ask: Can we combine both approaches to reduce *both* dynamic and static energy?

To answer this question, we study how *execution schedules* impact the time and energy consumption of large model training (§3). We define an *execution schedule* as the combination of three factors: (1) the *timing* of when communication kernels are launched within a sequence of computation kernels, (2) the *number of GPU Streaming Multiprocessors (SMs)* allocated to communication kernels, and (3) the *GPU frequency*.

We demonstrate that these factors *jointly* and *interdependently* determine time and energy consumption. Different execution schedules lead to different time and energy consumption—varying by as much as 3.29×—while the total amount of work remains the same. The optimal schedule is achieved by carefully balancing the resource consumption of computation and communication kernels, which depends on the interplay of all three factors. Crucially, *the best SM allocation and kernel launch timing depend on GPU frequency*—even for the same sequence of kernels, we cannot use the same SM allocation and launch timing at different frequencies. Existing solutions for kernel scheduling [17, 37, 42] and frequency scaling [15] optimize different subsets of these factors, and combining them naively is suboptimal for pushing the time–energy tradeoff frontier.

Based on these observations, we present *Kareus*, an energy-efficient large model training system that automatically finds the best execution schedule by jointly optimizing SM allocation, launch timing, and GPU frequency (§4.1). For all kernels on and off the critical path, it identifies the right number of SMs for communication and amount of computation–communication overlap, both in a frequency-specific manner. A collateral benefit is that the critical path itself becomes shorter due to improved overlap, reducing training time and shifting the entire time–energy tradeoff frontier.

Unfortunately, jointly optimizing all three factors via exhaustive search is impractical. The search space is prohibitively large for profiling each configuration. Worse, profiling heats up the GPU; without sufficient cooling intervals, one configuration’s measurement affects subsequent ones.

Kareus addresses these challenges by introducing the *partitioned overlap* execution model (§4.2). The execution graph for each forward and backward function is divided into fixed partitions, decomposing the global optimization problem into local subproblems. Partitioned overlap generalizes recent *nanobatching* techniques [17, 37, 42] and adds fine-grained control over all three factors, enabling precise control over the overlap between each communication kernel and its surround-

ing computation. For each partition, Kareus uses a multi-pass multi-objective optimization algorithm to identify candidates on the time–energy tradeoff frontier (§4.3). It then hierarchically composes local (partition-level) frontiers into a global (iteration-level) one for the entire training iteration (§4.4).

We implement Kareus by integrating with Perseus [15] and Megatron-LM [26] (§5). Kareus’s optimizer is informed by time and energy profiling results from our *thermally stable* profiler, which minimizes thermal interference between different configurations during profiling. Once the best execution schedule is identified, Kareus interacts with Perseus and Megatron-LM to enforce it for each forward and backward microbatch throughout the entire training execution.

We evaluate Kareus across 14 representative workloads, including real testbed training on Llama 3.2 3B and Qwen 3 1.7B, and large-scale emulation on Llama 3.3 70B (§6). Compared to the state-of-the-art Perseus, Kareus reduces energy by up to 28.3% under the same time budget, or reduces time by up to 27.5% under the same energy budget.

In summary, we make the following contributions:

- We show that SM allocation, launch timing, and GPU frequency jointly determine time and energy consumption, and that existing solutions optimizing subsets of these factors and naive combinations thereof are suboptimal.
- We design Kareus around the *partitioned overlap* execution model, decomposing the global optimization problem into tractable local subproblems.
- We evaluate Kareus on large model training workloads, demonstrating significant time and energy reduction compared to the state-of-the-art.

2 Background

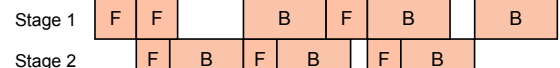
We begin by providing a brief background on GPU power consumption (§2.1). Then, we compare existing training systems in terms of their goals and techniques (§2.2), and discuss implications for training iteration time and energy (§2.3).

2.1 GPU Power Consumption

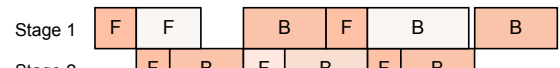
A GPU’s power consumption can be divided into two components: *dynamic power* and *static power*. Dynamic power is the power consumed by the chip’s *compute and memory activity*; it is proportional to core frequency and the square of voltage. In contrast, static power is consumed by *all parts of the chip* at all times regardless of utilization or activity; it largely does not depend on core frequency.

2.2 Existing Training Systems

Figure 1a illustrates Megatron-LM’s [26] implementation of the 1F1B pipeline schedule. Each pipeline microbatch (boxes labeled F and B) contains multiple Transformer [36] blocks, each with an Attention layer and a feed-forward (MLP) layer. Figure 2a shows the sequential kernel execution model adopted by the baseline Megatron-LM [26], where kernels execute one after another following data dependencies.

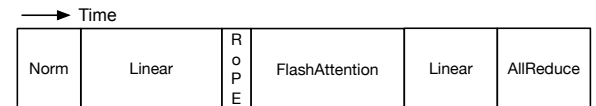


(a) *IF1B pipeline with no frequency scaling*

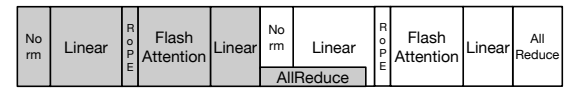


(b) *IF1B pipeline with frequency scaling by Perseus*

Figure 1: Existing training systems running the IF1B pipeline schedule [26]. Reder colors indicate higher GPU frequency and power draw. (a) The baseline Megatron-LM [26] does not perform any frequency scaling, whereas (b) Perseus [15] scales GPU frequencies of non-critical forward and backward computations to reduce energy consumption while maintaining the same latency.



(a) *Sequential kernel execution*



(b) *Nanobatching*

Figure 2: Transformer [36] Attention layer with tensor parallelism run with different execution models. (a) The sequential kernel execution model only runs one kernel at a time strictly following data dependencies. (b) Nanobatching [17, 37, 42] splits a pipeline microbatch into two nanobatches (illustrated with different colors) and staggers their execution, creating opportunities to overlap communication and computation.

Beyond parallelizing work across devices [6, 14, 20, 40], recent works have successfully optimized training time with *nanobatching* [17, 37, 42], where a single pipeline microbatch is split into two independent *nanobatches*. This creates opportunities to overlap communication and computation kernels from different nanobatches, as shown in Figure 2b, because there are no data dependencies between different nanobatches.

Finally, another line of work has optimized the energy consumption of large model training by scaling GPU frequencies [13, 15, 39]. Notably, Perseus [15] dynamically reduces the GPU frequencies of microbatches that are off the critical path of computation, as shown in Figure 1b, to reduce energy consumption while keeping overall training iteration time the same. However, it follows the sequential kernel execution model (Figure 2a), missing opportunities from fine-grained kernel scheduling like nanobatching.

2.3 Breaking Down Training Energy Consumption

We can better understand the impact of existing training systems and techniques on energy consumption by breaking down energy into static and dynamic components. Table 1 presents such a breakdown along with iteration time for Qwen

	Iteration time	Static energy	Dynamic energy	Total energy
Megatron-LM	5.60	5,372	21,374	26,745
Megatron-LM + Perseus	5.60	5,374	19,531	24,905
Nanobatching	5.31	5,096	21,445	26,541
Nanobatching + Perseus	5.37	5,160	19,729	24,889

Table 1: Training iteration time (seconds) and energy breakdown (Joules) of Megatron-LM, Nanobatching, and each combined with Perseus, training Qwen 3.1.7B on 16 NVIDIA A100 GPUs.

3.1.7B [34] training on 16 NVIDIA A100 GPUs.¹ Static energy is static power² multiplied by iteration time, and dynamic energy is static energy subtracted from total energy.

Compared to the baseline Megatron-LM (first row), Nanobatching (third row) reduces iteration time, which directly lowers static energy. In contrast, dynamic energy is also slightly higher because nanobatching may incur additional memory accesses, and will perform extra gradient accumulations for each nanobatch. Perseus applied to Megatron-LM (second row) reduces dynamic energy through explicit frequency scaling while keeping iteration time nearly the same, so static energy remains unchanged. Applying Perseus on top of Nanobatching (fourth row) combines both benefits: reduced static energy from shorter time and reduced dynamic energy from frequency scaling.

Is applying Perseus on top of Nanobatching the best we can do? To answer this, we first analyze how communication and kernel scheduling impact energy consumption (§3). This analysis reveals larger opportunities and informs our design of Kareus, which jointly optimizes kernel scheduling and frequency scaling (§4).

3 Energy Impact of Execution Schedules

We investigate the relationship between energy consumption and execution schedule. We first discuss how different execution schedules for the same *work* can lead to different energy consumption (§3.1), and then analyze the impact of key factors through case studies (§3.2). Table 2 summarizes key observations in this section.

3.1 Execution Schedule and Energy Consumption

Regardless of *how* work (computation, memory access, and communication) is performed, the total amount of work done is the same. How, then, can different execution schedules lead to different energy consumption?

The distinction between dynamic and static power is key to understanding this. Dynamic energy reflects the total work done on the hardware (i.e., transistors switching from computation, memory access, and communication). At *the same GPU frequency*, it remains largely constant across execution

¹The model is trained with microbatch size 16, 8 microbatches, and sequence length 4K, using pipeline parallelism degree 2, context parallelism degree 2, and tensor parallelism degree 4.

²Static power is set to be the GPU’s power draw when it is in *ready* state (power state P0) without running any significant computations.

schedules. In contrast, all parts of the hardware consume static power as long as they are powered on. Compute components (e.g., SMs) account for a significant portion of chip area and thus static power. When GPU resources are underutilized, static power is still dissipated without as much useful work being done, increasing total energy consumption.

In sum, GPU frequency mainly influences dynamic energy, whereas execution schedules influence resource utilization and thus static energy.

3.2 Interdependent Factors in Execution Schedules

We examine the time and energy consumption of different execution schedules induced by varying three key factors: (1) communication kernel launch timing, (2) number of SMs allocated to the communication kernel, and (3) GPU frequency. This definition of execution schedule generalizes nanobatching. The original nanobatching model (1) launches communication kernels as soon as possible, (2) uses default communication kernels like NCCL optimized for sequential execution (using excessive SMs assuming no concurrent kernels), and (3) ignores GPU frequency scaling.

Figure 3 shows the timelines and total energy consumption of different execution schedules for a single Transformer Attention layer of Llama 3.2 3B [24], with tensor parallelism degree 4 on four fully-connected NVIDIA A100 GPUs.³ We adopt the thermally stable profiling methodology described in Section 5.3. For simplicity of exposition, we focus on a single repeating segment: the computation kernels of one nanobatch and the communication kernel of the previous nanobatch. Note that there are no data dependencies between the communication kernel and the computation kernels within the segment. This is the common-case execution pattern throughout training.

3.2.1 SM Allocation

First, we study the impact of GPU resource sharing via SM allocation. Figures 3a, 3b, and 3c show execution schedules that vary only in the number of SMs allocated to the communication kernel (2, 4, and 20 SMs, respectively) while launching the communication kernel together with Linear 1. With two SMs allocated to the communication kernel (Figure 3a), it does not complete before all the computations finish, leading to an exposed communication period where 106 SMs are idle. This leads to static power wastage during the exposed communication time, which increases total energy consumption. As we increase the number of SMs to four (Figure 3b), the communication kernel completes before the computation kernels, leading to minimal static power wastage and total energy consumption. However, if we further increase the number of SMs to twenty (Figure 3c), while communication does speed up, it does so at the cost of taking away SMs from Linear 1, which ultimately increases total time and energy consumption. In other words, excess SMs allocated to the communication

³The batch size is 8 and the sequence length is 4K.

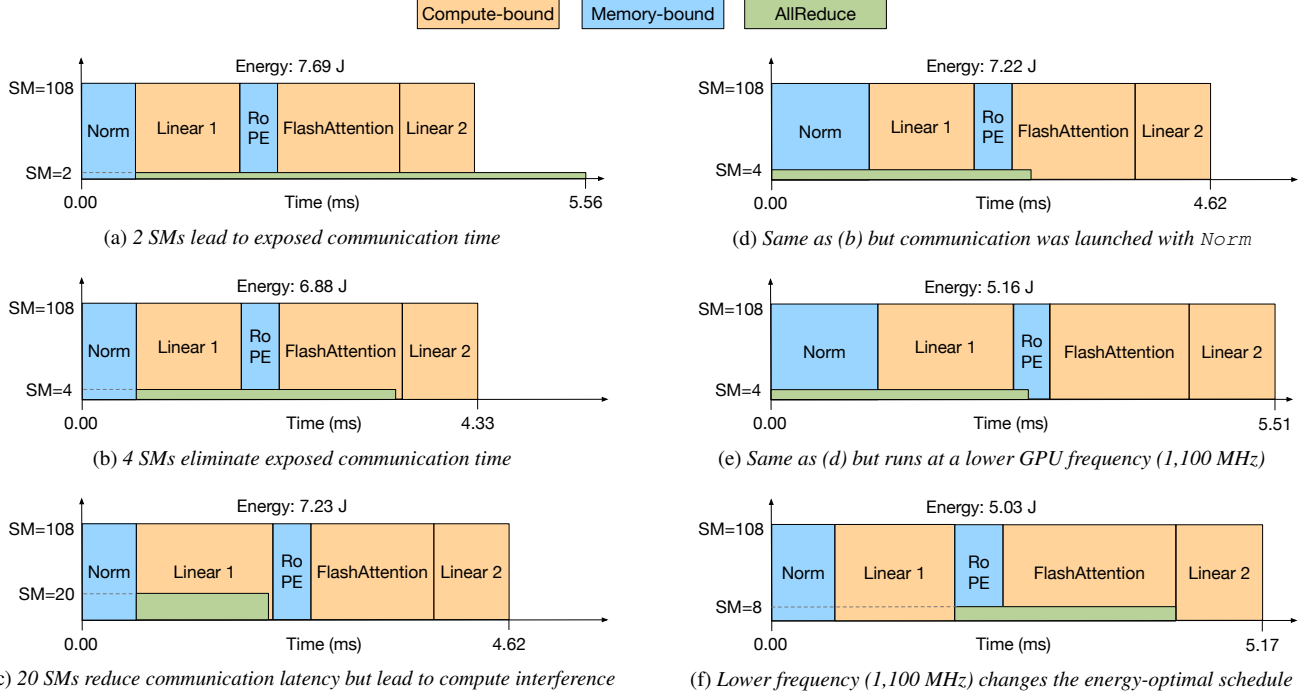


Figure 3: The time and total energy consumption of execution schedules for one Transformer Attention layer forward pass with varying SM allocation, communication launch timing, and GPU frequency. (a)–(c) show the effect of allocating different numbers of SMs to the communication kernel at 1,410 MHz, with (b) being the energy-optimal schedule. (d) is the same as (b), except that communication was launched earlier together with Norm. Finally, (e) and (f) run at a lower GPU frequency of 1,100 MHz. (e) is the same as (d) other than frequency, whereas (f) is the energy-optimal schedule at 1,100 MHz, which is different from the schedule in (b).

kernel only slows down computation while being practically close to idle themselves, again leading to increased static power wastage.

3.2.2 Communication Launch Timing

Next, we study the impact of the types of kernels that run together by changing when to launch the communication kernel. Figure 3d shows an execution schedule where the communication kernel runs with four SMs (the same as Figure 3b) but starts with Norm instead of Linear 1. As shown in colors, Norm and RoPE kernels are memory-bound, whereas, with sufficient SMs, the communication kernel also requires high memory bandwidth to write the communicated data to memory. When communication, which is also memory-heavy, starts together with a memory-bound kernel like Norm, both kernels compete for memory bandwidth, leading to longer execution time for both. This prolongs the period where compute resources are underutilized, wasting static power. Worse, during the execution of FlashAttention, some part of the HBM memory bandwidth is not utilized, which results in static power wastage from the HBM side.

3.2.3 Varying GPU Frequency

Finally, we study the impact of changing the GPU frequency. Reducing GPU frequency lowers dynamic energy [15, 39]. More importantly, the energy-optimal execution schedule

changes at lower frequencies. This is because at lower frequencies, all kernels become relatively more compute-bound, because reducing frequency only affects computation throughput and not memory throughput [29].⁴ Thus, running the communication kernel with a memory-bound kernel causes less interference since memory bandwidth is less contested. Conversely, running it with a compute-bound kernel and taking away SMs from it causes more severe interference, leading to larger slowdowns and static power wastage.

Figure 3e is the same as Figure 3d, but runs at a lower frequency (1,100 MHz). Reduced dynamic energy contributes a lot to lower total energy. However, execution time increases significantly because the communication kernel takes SMs away from Linear 1, which is now even more compute-bound at the lower frequency. The energy-optimal schedule at this frequency is shown in Figure 3f, which launches communication together with RoPE. This allows the compute-bound Linear kernels to run without interference, reducing total execution time and static power wastage.

Additionally, we note that exposed communication time is relatively more harmful at lower frequencies. Dynamic power decreases with frequency while static power remains constant—this increases static power’s proportion in total power draw and thus its relative impact when wasted.

⁴Essentially, the hardware roofline model’s horizontal compute-bound ceiling is lowered, making it easier for kernels to be compute-bound.

Factor	Observation	Explanation
SM allocation	A middle-ground sweet spot exists	Too few SMs for a kernel can lead to periods where only one small kernel is running, wasting static power; too many SMs slow down other kernels without significantly speeding up the target kernel.
Launch timing	Resource demands of kernels running together matter	Communication, which can be memory-bound, running together with memory-bound operations (e.g., Norm, RoPE) causes bandwidth contention and slowdown for everyone.
GPU frequency	Changes relative kernel resource demands	Lower frequency makes kernels relatively more compute-bound, changing which kernels benefit from overlapping; it also amplifies static power’s relative impact, making exposed communication more harmful.
All three	Time & energy impact of all factors are interdependent	The energy-optimal SM allocation and launch timing depend on the GPU frequency; changing one factor shifts the energy-optimal configurations of the others.

Table 2: Summary of factors and observations from case studies on the energy impact of execution schedules.

3.2.4 Joint Control and Opportunities

Table 2 summarizes the observations from the case studies above. The three factors that determine the execution schedule—SM allocation, communication launch timing, and GPU frequency—are (1) interdependent: changing one shifts the energy-optimal configuration of the others, and (2) highly impactful, with up to a $3.29\times$ gap in time and energy consumption among the observed schedules. Therefore, optimizing time and energy requires *joint control* of all three—this is the key insight that motivates the design of Kareus’s optimization algorithm.

In fact, joint control of GPU frequency and kernel scheduling is provably more energy-efficient than leaving GPU frequency control to the hardware’s power controller.

Theorem 1. *GPU frequency locked to the average frequency of a dynamic frequency schedule consumes less total energy.*

This is because dynamic power draw is proportional to frequency cubed, so moments when frequency is higher increase dynamic energy consumption super-linearly, whereas moments when frequency is lower reduce dynamic energy consumption only sub-linearly. Appendix A provides a proof.

Our analysis also shows that opportunities for energy savings with execution schedule control are significant. For simplicity of analysis we have studied a single Attention layer with modest communication volume (tensor parallelism degree 4). However, even in this setting, without any GPU frequency scaling, the energy-optimal execution schedule (Figure 3b) reduces energy consumption by 24.3% and time by 12.3% compared to the baseline Megatron-LM, and 7.1% energy and 5.4% time compared to Nanobatching. Larger models, more GPUs, and additional parallelism dimensions (e.g., context parallelism) provide even greater opportunities, as we show in Section 6.

4 Algorithm Design

In this section, we present the optimization algorithm of Kareus, whose goal is to find the time–energy tradeoff frontier of executing computation and communication kernels of large model training. We begin by formulating the optimization problem (§4.1), and then introduce the partitioned overlap execution model, which decomposes the problem

into tractable subproblems (§4.2). Building on this model, Kareus efficiently explores the execution schedule space to derive the time–energy frontier for each subproblem (§4.3), and then composes these local frontiers into a global frontier that characterizes the training iteration (§4.4). Finally, we discuss how Kareus generalizes to broader computation and communication patterns (§4.5).

4.1 Optimization Formulation

Objective. Prior works [15, 39] have shown the value of characterizing time–energy tradeoff frontiers, which allows users to select tradeoff points that meet job-level requirements (e.g., time deadlines, energy budgets) or perform dynamic adaptation to changing environments (e.g., stragglers). Particularly for large model training, the training iteration time–energy frontier can be constructed by combining the frontiers of each forward and backward microbatch in each pipeline stage [15]. Therefore, the goal of Kareus is to find a *microbatch* time–energy frontier: one that dominates frontiers established by prior works.

Decision variables. As explored in Section 3, three key factors influence the time and energy, which are the decision variables: (1) GPU frequency, (2) number of SMs to use for communication kernels, and (3) kernel launch timing which determines the execution order and overlap between kernels while keeping data dependencies.

Solution space. Unfortunately, the combined solution space of these three factors is extremely large. Using a typical Transformer-based LLM on an A100 GPU as an illustrative example, this space comprises 85,050 candidate configurations (details in Appendix B). This large search space is exacerbated by the lengthy profiling needed for accurate energy measurements (e.g., 13 seconds per candidate) for thermal stability (§5). With 85,050 candidates, exhaustive search can take up to 307 hours or 4,912 GPU-hours, which is impractical.

4.2 Partitioned Overlap Execution Model

Solving the global optimization problem directly is challenging due to its large search space, so we find *repeating patterns* in computation and communication sequences that can be independently optimized and composed into a global schedule.

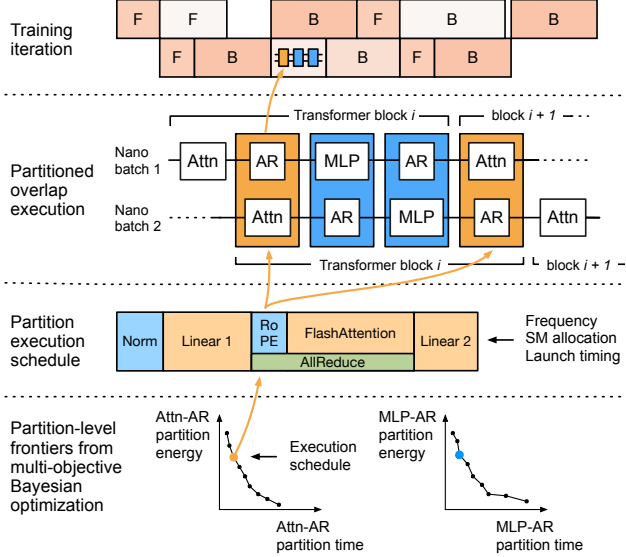


Figure 4: Kareus execution and optimization overview. The first row shows one training iteration with the 1F1B pipeline schedule. Inside each microbatch, partitions are sequentially executed; the second row illustrates this with the Transformer forward pass with tensor parallelism. The third row shows the execution schedule of the Attention–AllReduce partition. Each partition’s execution schedule is chosen from the partition-level time–energy frontiers (fourth row) characterized by Kareus’s optimization algorithm.

Partition. Kareus calls the set of kernels executing in repeating patterns a *partition*, defined as one communication kernel from a nanobatch with all computation kernels from the other nanobatch that *does not* have data dependencies with the communication kernel; they do not need to wait for the communication to complete, nor does the communication need to wait for them to complete. This allows the communication kernel to be overlapped with any contiguous sequence of computation kernels in the partition. The second row of Figure 4 illustrates this. The two orange boxes (Attention–AllReduce partition) are identical to each other, as well as the two blue boxes (MLP–AllReduce partition), and both types of partitions are shared across all Transformer blocks.

Optimization overview. After automatically detecting the partition definitions, Kareus’s optimizer first characterizes the time–energy frontier of each partition (§4.3), as shown in the fourth row of Figure 4. Each point on the frontier represents an efficient execution schedule for that partition, like the one depicted in the third row of Figure 4. Then, the time–energy frontiers of all partitions are combined to form the time–energy frontier of each forward and backward microbatch, and then combined again to form the global, iteration-level time–energy frontier (§4.4).

4.3 Multi-Objective Bayesian Optimization

Why Bayesian Optimization? For a single partition, our optimization problem still involves a complex search space

with mixed discrete and categorical variables. Importantly, the time and energy consumption of each configuration (1) is not a known analytical function of configuration values, and (2) can only be obtained through *costly* profiling. Bayesian Optimization (BO) is well-suited to this setting. It is capable of optimizing objectives over complex search spaces with typically up to 20 dimensions, where the objective is unknown in functional form and is costly to evaluate [18].

Adapting Bayesian Optimization. Applying BO directly to our setting is still non-trivial. Most crucially, our optimization problem is *multi-objective*—we aim to find the Pareto frontier of time and energy, while standard BO typically targets a single objective. Therefore, we design a Multi-objective Bayesian Optimization (MBO) algorithm tailored to our problem setting. In the following, we outline the overall flow of Bayesian Optimization, and then describe the design of each essential component tailored to our multi-objective setting.

Overall Bayesian Optimization flow. There are two key components in a BO algorithm. First, a *surrogate model* is trained on evaluated candidates to approximate the objective function. The surrogate model is initialized with random candidates and updated as new ones are evaluated. Second, *how to select next candidates* to evaluate is typically guided by an *acquisition function* that uses the surrogate model to rank candidates by how worthwhile they are to evaluate next.

With these components, BO proceeds in an iterative loop. It selects a batch of candidates using the acquisition function, evaluates them, updates the surrogate model, and repeats until convergence or a sample budget is reached. We describe how each component is designed in Kareus below.

Surrogate model. We adopt gradient-boosted decision trees (XGBoost) [10] as the surrogate model for two reasons. First, XGBoost training scales linearly with data points (versus cubic for Gaussian Processes), allowing fast retraining. Second, its tree-based structure handles discrete (GPU frequencies and SM allocations) and categorical (launch timing) parameters well. Due to this, XGBoost has been successfully adopted by kernel tuning frameworks (e.g., AutoTVM [11]).

We train two surrogate models: $\hat{T}(x)$ for time and $\hat{E}(x)$ for dynamic energy,⁵ where x is a candidate configuration. Since time is mainly influenced by SM allocation and launch timing and dynamic energy by GPU frequency, the two models are largely orthogonal. With these, total energy consumption can be computed as $\hat{T}(x) \cdot P_{\text{static}} + \hat{E}(x)$, where P_{static} is the GPU’s static power consumption.

Multi-pass candidate selection. Unlike typical BO that produces a single solution minimizing one objective, our MBO aims to find solutions on the time–energy Pareto frontier. Therefore, we design a *multi-pass* candidate selection procedure. Specifically, at each iteration of MBO, we select a batch of k candidates to evaluate next. The batch consists

⁵We use the hat notation to denote predictions, not true measurements.

of candidates selected based on multiple different acquisition functions, described below, that are designed to (1) cover complementary regions of the time–energy tradeoff space and (2) perform both exploration and exploitation to avoid over- or under-exploring certain regions.

Exploitation with hypervolume improvement.

The acquisition functions for exploitation are based on the concept of *hypervolume improvement* (HVI), which quantifies how much a candidate can expand the current time–energy frontier toward lower time and energy, as shown in Figure 5. It can be computed with

$$\text{HVI}(x) = \text{HV} \left(\mathcal{P} \cup \left\{ \left(\hat{T}(x), \text{Energy}(x) \right) \right\}; r \right) - \text{HV}(\mathcal{P}; r)$$

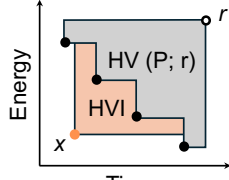


Figure 5: HVI.

where \mathcal{P} is the current set of candidates on the time–energy efficient frontier, and r is the reference point set to be slightly worse (outward) than the worst observed points, which is needed for the hypervolume (HV) to be computable. Given this, by switching the definition of $\text{Energy}(x)$ to be one of total energy, dynamic energy, or static energy, each derived (or, taken as is) from surrogate models $\hat{T}(x)$ and $\hat{E}(x)$, we obtain three HVI acquisition functions. Each acquisition function guides frontier expansion toward a distinct direction: dynamic energy favors lower-frequency candidates, static energy favors faster candidates, and total energy in the middle.

Exploration with uncertainty. An uncertainty-based acquisition function is needed to reduce the risk of under-exploring certain regions of the search space. We quantify uncertainty with *bootstrap ensembles*: multiple surrogate models trained on resampled datasets. The degree of *disagreement* between the surrogate models serves as a proxy for uncertainty (i.e., how unconfident we are about the prediction). Given that the goal of our uncertainty pass is to promote exploration, we use the sum of standard deviations (not variances) to prioritize candidates with high uncertainty in either objective.

The full picture. Figure 6 illustrates frontier expansion for the Llama 3.2 3B model’s MLP–AllReduce partition.⁶ Each pass expands the frontier in a direction aligned with its acquisition function, producing a more complete frontier than any single pass alone. Further, Algorithm 1 summarizes the overall Kareus MBO procedure for one partition. The optimization of each partition is independent. Appendix C provides detailed settings of hyperparameters including initial random sample size, batch size, ensemble size, and stopping criteria.

⁶The batch size is 4 and the sequence length is 4096, with tensor parallelism degree 8. We plot the time–energy frontier used in frontier composition algorithm in Section 4.4, which is the dynamic energy frontier.

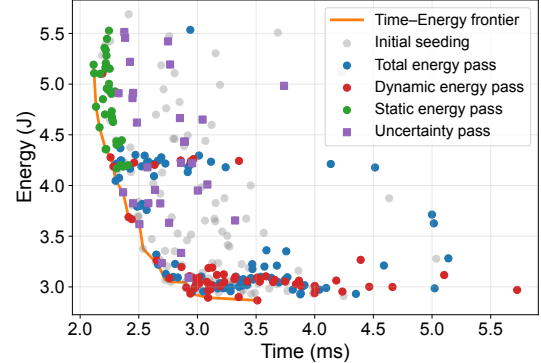


Figure 6: Multi-pass MBO in action with the Llama 3.2 3B model’s MLP–AllReduce partition. The three exploitation passes (total energy, dynamic energy, static energy) and the exploration pass expand the efficient frontier in complementary directions, as shown by the colors of the points that land on the time–energy frontier.

4.4 Composing Frontiers

With each partition’s time–energy frontier in hand, Kareus composes them to first form microbatch-level and then iteration-level frontiers.

From partition frontiers to microbatch frontier. A microbatch consists of multiple partitions executed sequentially. To construct the microbatch frontier, Kareus enumerates combinations of partition execution schedules (frequency, SM allocation, launch timing), sums their time and energy, and prunes suboptimal combinations to obtain the microbatch frontier. Algorithm 2 illustrates this process.

Two design decisions keep enumeration tractable. First, Kareus enforces a uniform GPU frequency across all partitions within a microbatch since frequency switching incurs several milliseconds of overhead, which is not negligible compared to partition latency. Second, partitions of the same type share the same SM allocation and launch timing. For instance, all Attention–AllReduce partitions in Figure 4 use identical configurations. Allowing per-partition configurations would explode the search space exponentially with the number of partitions with little benefit.

From microbatch frontiers to iteration frontier. The first row of Figure 4 shows an example of how forward (F) and backward (B) microbatches are scheduled across pipeline stages. Iteration time is the sum of microbatch latencies along the critical path, while iteration energy combines the energy of all microbatches plus static energy consumed during idle times. Kareus adopts Perseus’s iterative algorithm [15] to construct the training iteration frontier from microbatch frontiers.

4.5 Generalizations

Section 4.2 illustrated partitions using tensor parallelism as a running example. Real workloads, however, present more complex patterns that Kareus handles as follows.

Algorithm 1: Multi-pass multi-objective Bayesian Optimization for one partition

```

// Construct initial dataset for surrogate models
1  $\mathcal{D} \leftarrow N_{\text{init}}$  random candidates sampled and evaluated
2 for  $b = 1, 2, \dots, B_{\text{max}}$  do
3   Train surrogate models  $\hat{T}(x)$  and  $\hat{E}(x)$  on  $\mathcal{D}$ .
  // Exploitation: Hypervolume improvement
  foreach  $x \in \mathcal{X} \setminus \mathcal{D}$  do
    Compute  $\text{HVI}_{\text{tot}}(x)$ ,  $\text{HVI}_{\text{dyn}}(x)$ ,  $\text{HVI}_{\text{stat}}(x)$ .
  // Exploration: Uncertainty via bootstrap ensemble
  for  $m = 1$  to  $M$  do
    Train  $\hat{T}^m(x)$  and  $\hat{E}^m(x)$  on resampled  $\mathcal{D}$ 
  foreach  $x \in \mathcal{X} \setminus \mathcal{D}$  do
     $\text{Unc}(x) \leftarrow \sigma(\{\hat{T}^m(x)\}) + \sigma(\{\hat{E}^m(x)\})$ 
  // Multi-pass candidate selection
   $\mathcal{C} \leftarrow \text{TopK}(\{\text{HVI}_{\text{tot}}(x) : \forall x \in \mathcal{X} \setminus \mathcal{D}\}, k_1)$ 
   $\mathcal{C} \leftarrow \mathcal{C} \cup \text{TopK}(\{\text{HVI}_{\text{dyn}}(x) : \forall x \in \mathcal{X} \setminus \mathcal{D}\}, k_2)$ 
   $\mathcal{C} \leftarrow \mathcal{C} \cup \text{TopK}(\{\text{HVI}_{\text{stat}}(x) : \forall x \in \mathcal{X} \setminus \mathcal{D}\}, k_3)$ 
   $\mathcal{C} \leftarrow \mathcal{C} \cup \text{TopK}(\{\text{Unc}(x) : \forall x \in \mathcal{X} \setminus \mathcal{D} \setminus \mathcal{C}\}, k - |\mathcal{C}|)$ 
  // Evaluate candidates and update dataset
   $\mathcal{D} \leftarrow \mathcal{D} \cup \{(x, T(x), E(x)) : x \in \mathcal{C}\}$ 
  // Stopping condition
   $\Delta \leftarrow \text{Average HV improvement over } R \text{ batches}$ 
  if  $\Delta < \varepsilon$  then
    break
18 return  $\text{GetFrontier}(\mathcal{D})$ 

```

Multiple communication kernels. When consecutive communication kernels appear (e.g., multiple AllGather operations under context parallelism to aggregate key and value tensors [14, 24]), Kareus fuses them into a single kernel that shares an SM allocation. This reduces kernel launch overhead and keeps scheduling tractable. With this, any model and communication scheme reduces to alternating sequences of computations and a single (possibly fused) communication, fitting the partitioned overlap model.

Short consecutive memory-bound computations. When multiple short, memory-bound operations appear consecutively (e.g., BiasDropoutAdd followed by Norm), Kareus groups them into one logical operation. Treating them separately would increase the number of possible launch timings with only limited solution quality improvement.

Execution model switching. Partitioned overlap is not universally superior. When the amount of work within a microbatch is small (e.g., small models or small microbatch sizes), splitting the microbatch can reduce arithmetic intensity even more, leading to compute underutilization and higher static power wastage. In these cases, sequential execution can be more energy-efficient. To capture this, Kareus also profiles each sequentially executed microbatch at each frontier and includes them as candidates when constructing the microbatch

Algorithm 2: Microbatch frontier construction

```

1  $\mathcal{C} \leftarrow \emptyset$  // All feasible (time, energy) pairs for microbatch
2 foreach  $f \in \text{GPU frequencies}$  do
  // Cartesian product of configs across all partitions
   $\Theta \leftarrow \prod_{p \in \mathcal{P}} (\text{SM allocations} \times \text{launch timings})_p$ 
  foreach  $\theta \in \Theta$  do
    // Accumulate time and energy for microbatch
     $T_m \leftarrow 0, E_m \leftarrow 0$ 
    foreach  $\text{partition } p \in \mathcal{P}$  do
       $T_m \leftarrow T_m + T_p(f, \theta[p])$ 
       $E_m \leftarrow E_m + E_p(f, \theta[p])$ 
    foreach  $\text{non-partition component } c$  do
       $T_m \leftarrow T_m + T_c(f)$ 
       $E_m \leftarrow E_m + E_c(f)$ 
     $\mathcal{C} \leftarrow \mathcal{C} \cup \{(T_m, E_m)\}$ 
13 return  $\text{GetFrontier}(\mathcal{C})$ 

```

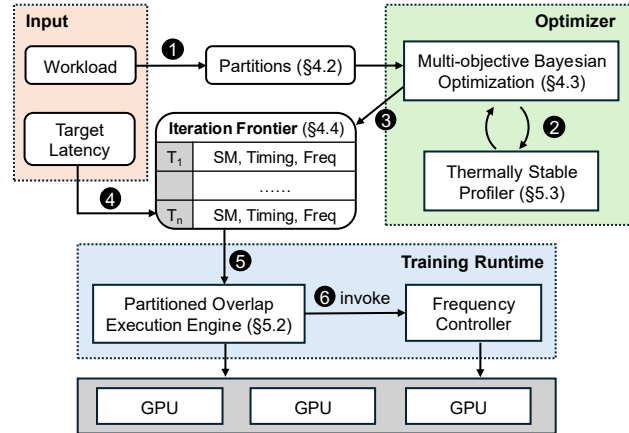


Figure 7: *Kareus system overview*.

time–energy frontier. Thus, the final microbatch frontier will automatically be constructed with the better execution model.

5 Implementation

5.1 System Overview

Figure 7 shows an overview of the Kareus system. Starting from a workload, Kareus automatically identifies partitions (1; §4.2), performs multi-objective Bayesian optimization per partition (2; §4.3), evaluating candidates with the thermally stable profiler (3; §5.3), and composes the iteration time–energy frontier (3; §4.4). Given a target iteration latency, Kareus selects execution schedules from the frontier (4) and deploys them to the partitioned overlap execution engine (5; §5.2), which invokes the GPU frequency controller to asynchronously switch each GPU’s frequency as planned (6).

5.2 Partitioned Overlap Execution Engine

Kareus’s training execution engine builds on Megatron-LM [26], executing Transformer blocks as a sequence of par-

titions. Before each microbatch execution, Kareus loads the corresponding microbatch configuration, switches between Megatron-LM’s default sequential execution and our partitioned overlap execution mode, and configures the SM allocation and launch timing for partitioned overlap execution. A custom `torch.autograd.Function` wraps all partitions of a Transformer block, allowing different partitions and partition schedules for forward and backward passes.

Communication kernels in Kareus are implemented with MSCCL++ [3, 31], which provides fine-grained SM allocation control with grid size. Computation and communication run on separate CUDA streams to enable overlap, and CUDA events control launch timing. GPU frequency is controlled with the Zeus Pipeline Frequency Optimizer [5, 15].

5.3 Thermally Stable Profiling

Kareus measures time and energy of a partition during MBO using Zeus [5, 39], which internally uses NVML [4]. We found that accurate energy measurements require care. The detailed experimental analysis is presented in Section 6.5.

Measurement window. NVML’s sampling interval on NVIDIA GPUs is approximately 100 ms, so millisecond-scale measurements incur large errors. Kareus executes each partition repeatedly over a 5-second window, as energy measurement becomes stable after several seconds.

Thermal cooldown. The power consumption of any hardware is temperature-dependent. Without cooldown between candidates, earlier profiles of another partition may heat up the GPU and bias subsequent measurements. Kareus inserts a 5-second cooldown period, which reliably brings the GPU below 32°C in our environment; the required duration depends on the server’s cooling capability.

In sum, profiling each candidate takes approximately 13 seconds in our setup, including initialization, warm-up, measurement, cooldown, and the synchronization between them.

6 Evaluation

We evaluate Kareus on 14 workloads and compare it against state-of-the-art baselines. Our key findings are as follows:

- Kareus achieves a superior time–energy frontier compared to prior approaches. In end-to-end training on real GPUs, it delivers up to 28.3% energy reduction under the same time budget and up to 27.5% time reduction under the same energy budget compared to the baselines (§6.2).
- In emulated large-scale training, Kareus consistently outperforms the baselines, achieving time and energy reductions comparable to real-world training results (§6.3).
- Kareus’s MBO algorithm constructs the time–energy frontier with reasonable overhead, and each pass in multi-pass candidate selection is indispensable (§6.4).

Table 3: Testbed experiment configurations. *TP* denotes tensor parallelism, and *CP* denotes context parallelism. Pipeline parallelism degree is fixed at 2, and number of microbatches is fixed at 8.

Model	Parallelism	Microbatch Size	Sequence Length
Llama 3.2 3B	TP8	8	4096
		8	8192
		16	4096
Llama 3.2 3B	CP2+TP4	8	4096
		8	8192
		16	4096
Qwen 3 1.7B	TP8	8	4096
		8	8192
		16	4096
Qwen 3 1.7B	CP2+TP4	8	4096
		8	8192
		16	4096

6.1 Experimental Setup

Testbed. Experiments are conducted on 16 NVIDIA A100 GPUs deployed across two AWS p4d.24xlarge instances. GPUs are fully connected intra-node via NVSwitch, and cross-node bandwidth is 400 Gbps.

Workloads. We evaluate Kareus on Llama 3.2 3B [24] and Qwen 3 1.7B [34] on the physical testbed, and perform large-scale emulation for Llama 3.3 70B [24]. For pipeline parallelism, we manually partition stages such that stages are as balanced as possible, following Perseus [15]. For context parallelism, we follow the scheme used in Llama 3 [24], where key–value tensors are collected across GPUs via AllGather. We use activation checkpointing to reduce memory pressure.

Baselines. We mainly compare against three baselines:

- **Megatron-LM (M).** Baseline Megatron-LM [26] with the sequential execution model and maximum GPU frequency. Produces a single point on the time–energy plane.
- **Megatron-LM + Perseus (M+P).** Perseus [15] applied to the above. This produces a time–energy frontier.
- **Nanobatching + Perseus (N+P).** A training engine based on Megatron-LM that implements nanobatching, a special case of Kareus’s partitioned overlap execution model (§3.2), integrated with Perseus like the above. This also produces a time–energy frontier.

Metrics. We adopt two modes of comparison based on two viable use cases. Figure 8 illustrates the metrics.

- **Max-throughput comparison.** When iteration time constraints (e.g., deadlines, stragglers) are not present, the training pipeline operates in maximum-throughput mode. For methods that produce a time–energy frontier, this means operating at the leftmost (lowest time) point. We set Megatron-LM as the baseline, and report iteration time and energy reduction (%) of M+P, N+P, and Kareus.

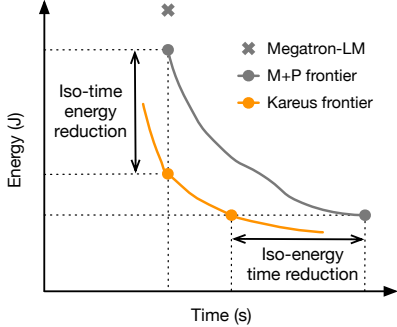


Figure 8: Toy example showing iteration time-energy frontiers. For the max-throughput comparison, we compare the leftmost points of each frontier with Megatron-LM. For frontier improvement, we report the iso-time energy reduction and iso-energy time reduction compared to Megatron-LM + Perseus.

- **Frontier improvement.** Simply comparing the leftmost point does not fully capture the benefits of a superior time-energy frontier. We set M+P as the baseline, and define two metrics that compare frontier improvements for N+P and Kareus: (1) *Iso-time energy reduction (%)*, energy reduction with iteration time deadline set as M+P’s minimum iteration time; and (2) *Iso-energy time reduction (%)*, time reduction with iteration energy budget set as M+P’s minimum iteration energy.

6.2 End-to-end Results

In this section, we evaluate the iteration time and energy performance on the testbed GPUs for the max-throughput (§6.2.1) and frontier improvement (§6.2.2) comparisons. The workload configurations (parallelism, microbatch size, and sequence length) can be found in Table 3.

6.2.1 Max-Throughput Comparison

Table 4 reports the iteration time and energy reductions achieved by all methods under the max-throughput regime. Overall, Kareus achieves up to 14.9% reduction in iteration time and 22.1% reduction in energy consumption compared to Megatron-LM, strictly outperforming the baselines on time and energy.

Time reduction. The time reduction mainly comes from reducing SM idle time caused by resource underutilization due to solo communication kernels or resource contention induced by poorly scheduled kernel overlaps. As a result, the time reduction trend largely follows the communication overhead induced by different model configurations. Compared to Megatron-LM, both overlap execution models achieve larger gains under tensor parallelism (TP) than under context parallelism with tensor parallelism (CP+TP). Moreover, increasing the batch size yields greater time reduction than increasing the sequence length, since the former introduces relatively higher communication overhead.

When compared to Nanobatching, Kareus provides larger additional gains under CP+TP than under TP alone, because

fine-grained control of communication scheduling becomes more critical for complex communication patterns. Moreover, Nanobatching can significantly slow down computation (e.g., on Qwen 1.7B with CP2+TP4, batch size 8, and sequence length 4K), as it leads to SM underutilization when the workload is small. In contrast, Kareus can automatically switch to the sequential execution model (§4.5).

Energy reduction. Energy reflects the combined effects of time and power. Therefore, the energy reduction trend does not always track the time reduction trend. In many cases, Nanobatching + Perseus reduces time but yields smaller energy reduction than Megatron-LM + Perseus, because overlap raises SM utilization and thus also power, and the power increase offsets time reduction. In contrast, Kareus achieves larger energy reductions by simultaneously optimizing overlap and GPU frequency, which reduces both time and power.

Case study. We find an interesting case in Qwen 3 1.7B with TP8, batch size 8, and sequence length 4K. Both baselines operate the critical-path microbatch at 1,410 MHz (the maximum GPU frequency). However, Kareus discovers an overlap configuration that runs at 1,350 MHz yet attains the fastest latency, resulting in a 1.73× energy reduction over Nanobatching + Perseus. This happens because nanobatching overlap at 1,410 MHz improves resource utilization but raises instantaneous power, which triggers GPU frequency throttling. Thus, the time-averaged GPU frequency (which determines execution time) is close to 1,350 MHz, while the time-averaged dynamic power (which determines dynamic energy) remains closer to that of 1,410 MHz. In contrast, operating at a constant frequency is more energy-efficient than fluctuating frequency with the same average. This is a concrete instance of Theorem 1 in Section 3.2.4. This case highlights the importance of jointly optimizing kernel scheduling and GPU frequency scaling to minimize energy consumption.

Figure 9 illustrates representative partition execution schedules across microbatches for the above case⁷. In the Attention-AllReduce partition, Kareus prefers not to overlap AllReduce with memory-bound kernels (e.g., Norm) at a higher frequency (1,350 MHz), and instead shifts the overlap to more memory-bound kernels at a lower frequency (1,290 MHz), consistent with the analysis in Section 3. The selected configurations differ for the backward Attention-AllReduce and MLP-AllReduce partitions due to variations in kernel lengths and types. For example, the backward FlashAttention is long enough to overlap with AllReduce under an appropriate SM allocation. In contrast, in the MLP-AllReduce partition without FlashAttention, Kareus reduces SM allocation and overlaps from the beginning, which minimizes interference with other kernels.

⁷Consecutive memory-bound kernels are grouped and labeled as a single kernel. Backward microbatches are partitioned following the definition in Section 4.2; Norm is treated as the first kernel because it follows the AllReduce kernel in the transformer block, and other kernels are ordered in reverse.

Table 4: Iteration time and energy reductions (%) relative to Megatron-LM (higher is better) for all methods under the max-throughput configuration. Metrics are grouped by time and energy. OOM indicates that the GPU runs out of memory at the corresponding settings. Negative values indicate increased time or energy relative to the baseline.

Model	Parallelism	μ Batch Size	Sequence Length	Time Reduction (%)			Energy Reduction (%)		
				Megatron-LM +Perseus	Nanobatching +Perseus	Kareus	Megatron-LM +Perseus	Nanobatching +Perseus	Kareus
Llama 3.2 3B	TP8	8	4K	−0.3	8.5	12.3	10.0	15.5	19.6
		8	8K						
		16	4K						
Llama 3.2 3B	CP2TP4	8	4K	0.2	0.0	5.2	7.4	7.3	14.4
		8	8K						
		16	4K						
Qwen 3 1.7B	TP8	8	4K	−0.5	5.6	12.2	7.7	12.8	22.1
		8	8K						
		16	4K						
Qwen 3 1.7B	CP2TP4	8	4K	−0.5	−20.4	−0.5	7.1	3.1	7.1
		8	8K						
		16	4K						

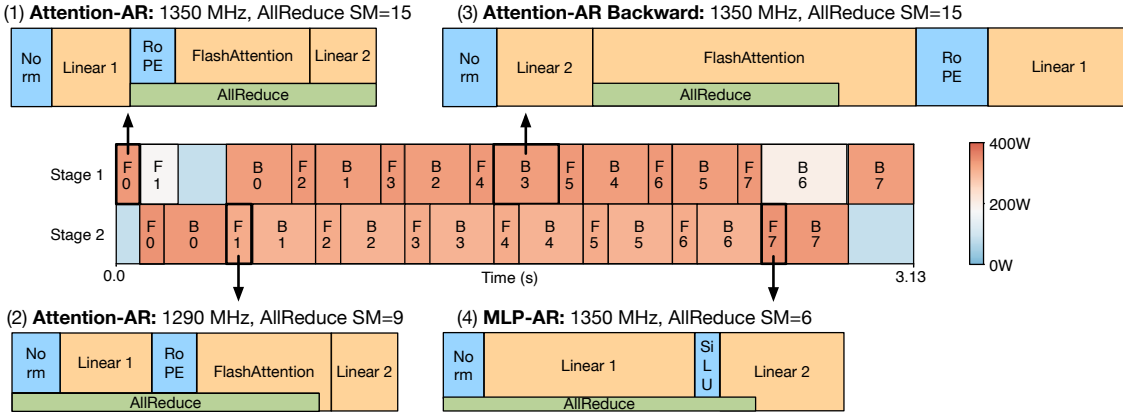


Figure 9: Case study of Qwen 3 1.7B with TP8, microbatch size 8, and sequence length 4K. The pipeline schedule is colored by average GPU power draw, and the partition execution schedules are drawn to scale. (1)–(2) compare the Attention–AllReduce partition at 1,350 MHz and 1,290 MHz, respectively. (3) and (4) show the backward Attention–AllReduce and MLP–AllReduce partitions at 1,350 MHz.

6.2.2 Frontier Improvement

Table 5 reports the iso-time energy reduction and iso-energy time reduction for Nanobatching + Perseus and Kareus, which demonstrate the expansion of the time–energy frontier. We present the complete frontier comparison plots for each model configuration in Appendix D.1. Overall, Kareus achieves up to 28.3% iso-time energy reduction and 27.5% iso-energy time reduction compared to Megatron-LM + Perseus, establishing a strictly better time–energy tradeoff over Nanobatching + Perseus.

Under the same time budget, where static energy is fixed, Kareus achieves higher SM utilization and can therefore execute at lower GPU frequencies to complete the workload, reducing dynamic energy consumption. Conversely, under the same energy budget, Kareus minimizes static energy wastage, allowing more energy to be allocated to dynamic execution at higher GPU frequencies to complete the workload faster.

6.3 Large-Scale Emulation

In this section, we conduct large-scale emulation of Llama 3.3 70B based on smaller-scale profiling on our testbed hardware. We compare Kareus with Megatron-LM + Perseus and report the same metrics as in Section 6.2. We use the emulator from Perseus [2]. The results show that the trends in time and energy reduction are consistent with the end-to-end evaluation on the testbed GPUs.

Methodology and parameters. For Kareus, we obtain the iteration-level time–energy frontier using the MBO algorithm described in Section 4, by composing partition-level frontiers. For Megatron-LM + Perseus, we profile the time and energy of each Transformer block using the same profiling methodology described in Section 5.3, and construct the iteration-level frontier. We perform strong scaling as we vary the number of GPUs (Table 6), while fixing the global batch size to 2048, which is adopted in the Llama 3 training [24]. We use pipeline parallelism degree 10 and tensor parallelism degree 8, with microbatch size 4 and sequence length 4096 [24].

Table 5: Iso-time energy reduction (%) and iso-energy time reduction (%) relative to Megatron-LM + Perseus for Nanobatching + Perseus and Kareus. “—” indicates that no configuration satisfies that constraint. For example, if Nanobatching + Perseus has a longer iteration time than Megatron-LM + Perseus at the leftmost point, then no iso-time point exists.

			Iso-Time Energy Reduction (%)		Iso-Energy Time Reduction (%)	
			N+P	Kareus	N+P	Kareus
3B	TP8	8 4K	21.0		24.3	18.9
		8 8K			OOM	
		16 4K			OOM	
3B	CP2TP4	8 4K	—		17.4	7.0
		8 8K	4.0		12.4	4.4
		16 4K	6.6		20.4	5.1
1.7B	TP8	8 4K	16.8		26.8	17.8
		8 8K	20.0		23.1	17.7
		16 4K	20.4		28.3	19.9
1.7B	CP2TP4	8 4K	—		0.0	—
		8 8K	—		15.0	—0.4
		16 4K	8.9		20.1	8.4
						19.7

Table 6: Strong scaling configurations for large-scale emulation.

# GPUs	# Pipelines	# Microbatches Per Pipeline	Global Batch Size
10240	128	16	
5120	64	32	
2560	32	64	2048
1280	16	128	

Max-throughput comparison. We report the max-throughput comparison results for Megatron-LM + Perseus and Kareus across different numbers of microbatches in Table 7, and plot the corresponding iteration-level time–energy frontiers in Appendix D.2. The energy reductions achieved by both methods are generally higher than those observed in the testbed experiments, because the larger number of pipeline stages and microbatches on non-critical paths can be slowed down to save dynamic energy. As the number of microbatches increases, the relative portion of pipeline bubbles during the warm-up and cooldown phases—which are normally reduced down to the lowest frequency—decreases, leading to a slight decrease in energy reduction. The time reduction achieved by Kareus is slightly lower than that of the TP=8 case in the testbed experiments, because a smaller microbatch size is used in this setting due to the GPU memory constraints.

Frontier improvement. We report the frontier improvement results for Kareus across different numbers of microbatches in Table 8. As the number of microbatches increases, the iso-time energy reduction improves, because the absolute iteration time grows, providing more slack for dynamic energy savings. In contrast, the iso-energy time reduction decreases, since static energy consumes a larger fraction of the fixed energy budget.

Table 7: [Emulation] Iteration time and energy reduction (%) relative to Megatron-LM of Megatron-LM + Perseus and Kareus under the max-throughput configuration for Llama 3.3 70B.

# Microbatches	Time Reduction (%)		Energy Reduction (%)	
	M+P	Kareus	M+P	Kareus
16	0.0	9.3	15.0	20.2
32	0.0	9.2	14.3	20.0
64	0.0	9.1	13.8	19.8
128	0.0	9.1	13.5	19.7

Table 8: [Emulation] Iso-time energy reduction (%) and iso-energy time reduction (%) relative to Megatron-LM + Perseus of Kareus for Llama 3.3 70B.

	# Microbatches			
	16	32	64	128
Iso-Time Energy Reduction (%)	11.6	14.1	15.3	15.1
Iso-Energy Time Reduction (%)	19.1	16.8	16.4	16.0

6.4 MBO Analysis

Overhead and breakdown. Before end-to-end training, Kareus performs MBO (§4.3) to obtain the time–energy frontier for each partition. In our testbed experiments, MBO for different partitions is conducted in parallel and takes 2 hours on average. This overhead is substantially lower than that of exhaustive search (307 hours, as discussed in Section 4.1), and is negligible compared to typical end-to-end training times (e.g., 54 days for Llama 3 [24]).

The MBO overhead is dominated by thermally stable profiling of candidates (§5.3), accounting for 97% of the total overhead, with 3% spent on the search algorithm. For a typical partition in our setting, which evaluates a batch of 32 candidates per MBO iteration, thermally stable profiling takes 6.9 minutes on average, while surrogate model training and acquisition function evaluation incur an overhead of 11 seconds on average.

Multi-pass candidate selection. We summarize the distribution of candidates selected into the final time–energy frontier by each pass of the MBO process across all partitions and all 14 workloads, including both testbed experiments and emulation. On average, random initialization contributes 35% of the selected candidates—they happen to be on the frontier. The other 65% of the selected candidates are discovered by the total energy pass, dynamic energy pass, static energy pass, and uncertainty pass, each 25%, 22%, 12%, and 6% of the selected candidates, respectively.

6.5 Thermally Stable Profiler

During MBO, Kareus adopts thermally stable profiling to measure the time and energy of each candidate (§5.3). We conduct an experimental study using the Attention–AllReduce partition of Llama 3.2 3B on 8 NVIDIA A100 GPUs⁸ to

⁸Batch size is 4 and sequence length is 4K, with tensor parallelism degree 8, running at 1,410 MHz.

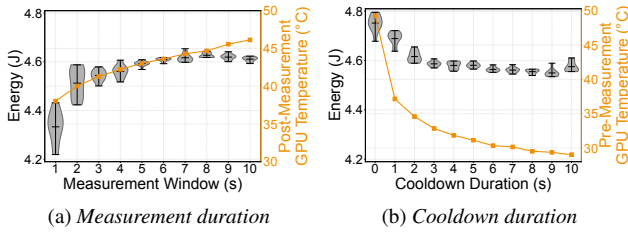


Figure 10: Impact of changing (a) measurement duration and (b) cooldown duration for the Thermally Stable Profiler. We report the distribution of energy across 10 repeated trials, along with the average GPU temperature before and after measurement.

analyze the impact of measurement window and cooldown duration on the energy measurement accuracy.

Measurement duration. We fix the cooldown duration to 5 seconds and vary the measurement window from 1 second to 10 seconds, each with 10 repeated profiling trials. Figure 10a shows the distribution of measured energy consumption under different measurement windows, together with the average GPU temperature *after* each measurement. With very short measurement windows (e.g., below 2 seconds), energy measurements exhibit large variability due to the 100 ms NVML counter update interval, and have a lower mean because the GPU has not fully warmed up. Energy measurement stabilizes from 5 seconds onward, which is why we chose 5 seconds as our measurement duration.

Cooldown duration. Cooldown duration is the waiting time between profiling consecutive partitions. We fix the measurement duration to 5 seconds and vary the cooldown duration from 0 second (no cooldown) to 10 seconds, with 10 repeated profiling trials. Figure 10b shows the distribution of measured energy consumption under different cooldown durations, along with the average GPU temperature *before* each measurement. We observe that mean energy consumption strongly correlates with the GPU temperature at the start of measurement, making sufficient cooldown essential for accurate measurement. Temperature and measurements stabilize from 5 seconds onward, so we cool down for 5 seconds between partitions.

7 Related Work

7.1 ML Energy Optimization

Energy consumption of ML workloads has attracted extensive attention, prompting a growing body of work on energy optimization [13, 15, 16, 32, 33, 39]. Particularly, the notion of the time–energy tradeoff frontier has been a key tool for reasoning about traditional performance and energy efficiency. For LLM serving, DynamoLLM [33] explores time–energy tradeoffs via model parallelism and GPU frequency scaling under latency constraints. The ML.ENERGY benchmark [16] characterizes the time–energy frontier across deployment configurations to guide latency-aware energy optimization. On

the training side, Zeus [39] identifies job-level time–energy tradeoffs on modest-scale workloads. Perseus [15] dynamically scales GPU frequency per microbatch to optimize energy under pipeline iteration time deadlines. However, these approaches often yield suboptimal frontiers as they overlook the impact of low-level execution scheduling, such as communication and computation overlap. Jayaweera et al. [22] propose energy-aware tile size selection for GPU kernels, but do not consider interactions with system-level latency targets, which limits the potential for energy optimization.

7.2 Communication Scheduling

As model scale grows, communication incurs increasingly significant overhead, motivating extensive work on overlapping communication with computation [8, 9, 12, 17, 21, 25, 27, 37, 38, 41, 42]. Nanobatching is a key technique that removes data dependencies and enables overlap opportunities. In LLM serving, NanoFlow [42] improves throughput via nanobatching with fine-grained kernel overlap. For training, DeepSpeed Domino [37] applies nanobatching to overlap tensor-parallel communication, while DeepSeek DualPipe [17] pipelines forward and backward nanobatches for communication overlap. Concerto [12] optimizes communication scheduling from a compiler perspective, and adopts partial nanobatching when under data dependencies. From the energy perspective, these approaches reduce static energy by reducing time, but do not explicitly optimize energy in their design. Kareus reveals the energy impact of communication scheduling, and generalizes the nanobatching strategy to enable fine-grained SM allocation and launch-timing control, further minimizing static energy, while jointly reducing dynamic energy by optimizing GPU frequency.

8 Conclusion

We present Kareus, an execution-aware energy optimizer for large model training. Kareus demonstrates that SM allocation, kernel launch timing, and GPU frequency jointly influence static and dynamic energy, and that the optimal time–energy frontier cannot be attained by optimizing them in isolation. Building on this insight, Kareus introduces a partitioned overlap execution model and a multi-objective Bayesian optimization framework that jointly searches over execution schedules, exposing a strictly better time–energy tradeoff frontier than prior systems.

Looking forward, we believe energy-aware execution scheduling should become a first-class concern in ML systems, not an afterthought. As AI scaling continues and energy constraints tighten for gigawatt-scale AI datacenters, systems that co-optimize computation, communication, and power will be essential—not just for cost savings, but for enabling training runs that would otherwise be infeasible. Kareus takes a step in this direction; we hope it spurs further work on energy as a core system design metric.

References

- [1] How much electricity does an American home use? <https://www.eia.gov/tools/faqs/faq.php?id=97&t=3>.
- [2] Lowtime. <https://github.com/ml-energy/lowtime>.
- [3] MSCCL++. <https://github.com/microsoft/mscclpp.git>.
- [4] NVIDIA Management Library (NVML). <https://developer.nvidia.com/nvidia-management-library-nvml>.
- [5] Zeus. <https://github.com/ml-energy/zeus>.
- [6] Sami Alabed, Daniel Belov, Bart Chrzaszcz, Juliana Franco, Dominik Grewe, Dougal Maclaurin, James Mollay, Tom Natan, Tamara Norman, Xiaoyue Pan, Adam Paszke, Norman A. Rink, Michael Schaarschmidt, Timur Situdikov, Agnieszka Swietlik, Dimitrios Vytiniotis, and Joel Wee. PartIR: Composing SPMD partitioning strategies for machine learning. In *ASPLOS*, 2025.
- [7] CBRE. Global data center trends 2025. <https://www.cbre.com/insights/reports/global-data-center-trends-2025>, 2025.
- [8] Li-Wen Chang, Wenlei Bao, Qi Hou, Chengquan Jiang, Ningxin Zheng, Yinmin Zhong, Xuanrun Zhang, Zuquan Song, Chengji Yao, Ziheng Jiang, Haibin Lin, Xin Jin, and Xin Liu. Flux: Fast software-based communication overlap on gpus through kernel fusion. *arXiv preprint arXiv:2406.06858*, 2024.
- [9] Chang Chen, Xiuhong Li, Qianchao Zhu, Jiangfei Duan, Peng Sun, Xingcheng Zhang, and Chao Yang. Centauri: Enabling efficient scheduling for communication-computation overlap in large model training via communication partitioning. In *ASPLOS*, 2024.
- [10] Tianqi Chen and Carlos Guestrin. XGBoost: A scalable tree boosting system. In *KDD*, 2016.
- [11] Tianqi Chen, Lianmin Zheng, Eddie Yan, Ziheng Jiang, Thierry Moreau, Luis Ceze, Carlos Guestrin, and Arvind Krishnamurthy. Learning to optimize tensor programs. In *NeurIPS*, 2018.
- [12] Shenggan Cheng, Shengjie Lin, Lansong Diao, Hao Wu, Siyu Wang, Chang Si, Ziming Liu, Xuanlei Zhao, Jiangsu Du, Wei Lin, and Yang You. Concerto: Automatic communication optimization and scheduling for large-scale deep learning. In *ASPLOS*, 2025.
- [13] Sangjin Choi, Inhoe Koo, Jeongseob Ahn, Myeongjae Jeon, and Youngjin Kwon. EnvPipe: Performance-preserving DNN training framework for saving energy. In *ATC*, 2023.
- [14] Weiwei Chu, Xinfeng Xie, Jiecao Yu, Jie Wang, Amar Phanishayee, Chunqiang Tang, Yuchen Hao, Jianyu Huang, Mustafa Ozdal, Jun Wang, Vedanuj Goswami, Naman Goyal, Abhishek Kadian, Andrew Gu, Chris Cai, Feng Tian, Xiaodong Wang, Min Si, Pavan Balaji, Ching-Hsiang Chu, and Jongsoo Park. Scaling llama 3 training with efficient parallelism strategies. In *ISCA*, 2025.
- [15] Jae-Won Chung, Yile Gu, Insu Jang, Luoxi Meng, Nikhil Bansal, and Mosharaf Chowdhury. Reducing energy bloat in large model training. In *SOSP*, 2024.
- [16] Jae-Won Chung, Jeff J. Ma, Ruofan Wu, Jiachen Liu, Oh Jun Kweon, Yuxuan Xia, Zhiyu Wu, and Mosharaf Chowdhury. The ML.ENERGY benchmark: Toward automated inference energy measurement and optimization. In *NeurIPS Datasets and Benchmarks*, 2025.
- [17] DeepSeek-AI. DeepSeek-V3 technical report. *arXiv preprint arXiv:2412.19437*, 2024.
- [18] Peter I. Frazier. A tutorial on bayesian optimization. *arXiv preprint arXiv:1807.02811*, 2018.
- [19] James Hamilton. Constraint-driven innovation (CIDR 2024 keynote talk). <https://mvdirona.com/jrh/talksandpapers/JamesHamiltonCIDR2024.pdf>.
- [20] Insu Jang, Runyu Lu, Nikhil Bansal, Ang Chen, and Mosharaf Chowdhury. Efficient distributed mllm training with cornstarch. *arXiv preprint arXiv:2503.11367*, 2025.
- [21] Abhinav Jangda, Jun Huang, Guodong Liu, Amir Hossein Nodehi Sabet, Saeed Maleki, Youshan Miao, Madanlal Musuvathi, Todd Mytkowicz, and Olli Saarikivi. Breaking the computation and communication abstraction barrier in distributed machine learning workloads. In *ASPLOS*, 2022.
- [22] Malith Jayaweera, Martin Kong, Yanzhi Wang, and David Kaeli. Energy-aware tile size selection for affine programs on gpus. In *CGO*, 2024.
- [23] Helen Kou. Power for AI: Easier said than built. <https://about.bnef.com/insights/commodities/power-for-ai-easier-said-than-built/>, 2025.
- [24] AI Meta Llama Team. The llama 3 herd of models. *arXiv preprint arXiv:2407.21783*, 2024.
- [25] Runyu Lu, Shiqi He, Wenxuan Tan, Shenggui Li, Ruofan Wu, Jeff J. Ma, Ang Chen, and Mosharaf Chowdhury.

Tetriserve: Efficient dit serving for heterogeneous image generation. In *ASPLOS*, 2026.

[26] Deepak Narayanan, Mohammad Shoeybi, Jared Casper, Patrick LeGresley, Mostafa Patwary, Vijay Korthikanti, Dmitri Vainbrand, Prethvi Kashinkunti, Julie Bernauer, Bryan Catanzaro, Amar Phanishayee, and Matei Zaharia. Efficient large-scale language model training on GPU clusters using Megatron-LM. In *SC*, 2021.

[27] Suchita Pati, Shaizeen Aga, Mahzabeen Islam, Nuwan Jayasena, and Matthew D. Sinclair. T3: Transparent tracking & triggering for fine-grained overlap of compute & collectives. In *ASPLOS*, 2024.

[28] David Patterson, Joseph Gonzalez, Quoc Le, Chen Liang, Lluis-Miquel Munguia, Daniel Rothchild, David So, Maud Texier, and Jeff Dean. Carbon emissions and large neural network training. *arXiv preprint arXiv:2104.10350*, 2021.

[29] Ryan Prescott. Advanced API performance: SetStablePowerState. <https://developer.nvidia.com/blog/advanced-api-performance-setstablepowerstate/>, 2022.

[30] SemiAnalysis. InferenceMAX: Open source inference benchmarking. <https://newsletter.semanalysis.com/p/inferencemax-open-source-inference>, 2025.

[31] Aashaka Shah, Abhinav Jangda, Binyang Li, Caio Rocha, Changho Hwang, Jithin Jose, Madan Musuvathi, Olli Saarikivi, Peng Cheng, Qinghua Zhou, Roshan Dathathri, Saeed Maleki, and Ziyue Yang. Mscl++: Rethinking gpu communication abstractions for cutting-edge ai applications. *arXiv preprint arXiv:2504.09014*, 2025.

[32] Jovan Stojkovic, Chaojie Zhang, Íñigo Goiri, Esha Choukse, Haoran Qiu, Rodrigo Fonseca, Josep Torrellas, and Ricardo Bianchini. Tapas: Thermal- and power-aware scheduling for llm inference in cloud platforms. In *ASPLOS*, 2025.

[33] Jovan Stojkovic, Chaojie Zhang, Inigo Goiri, Josep Torrellas, and Esha Choukse. DynamoLLM: Designing llm inference clusters for performance and energy efficiency. In *HPCA*, 2025.

[34] Qwen Team. Qwen3 technical report. *arXiv preprint arXiv:2505.09388*, 2025.

[35] U.S. Energy Information Administration (EIA). Capital cost and performance characteristics for utility-scale electric power generating technologies. <https://www.eia.gov/analysis/studies/powerplants/> capitalcost/pdf/capital_cost_AEO2025.pdf, 2024.

[36] Ashish Vaswani, Noam Shazeer, Niki Parmar, Jakob Uszkoreit, Llion Jones, Aidan N. Gomez, Łukasz Kaiser, and Illia Polosukhin. Attention is all you need. In *NeurIPS*, 2017.

[37] Guanhua Wang, Chengming Zhang, Zheyu Shen, Ang Li, and Olatunji Ruwase. Domino: Eliminating communication in llm training via generic tensor slicing and overlapping. *arXiv preprint arXiv:2409.15241*, 2024.

[38] Shibo Wang, Jinliang Wei, Amit Sabne, Andy Davis, Berkin Ilbeyi, Blake Hechtman, Dehao Chen, Karthik Srinivasa Murthy, Marcello Maggioni, Qiao Zhang, Sameer Kumar, Tongfei Guo, Yuanzhong Xu, and Zongwei Zhou. Overlap communication with dependent computation via decomposition in large deep learning models. In *ASPLOS*, 2022.

[39] Jie You, Jae-Won Chung, and Mosharaf Chowdhury. Zeus: Understanding and optimizing GPU energy consumption of DNN training. In *NSDI*, 2023.

[40] Lianmin Zheng, Zhuohan Li, Hao Zhang, Yonghao Zhuang, Zhifeng Chen, Yanping Huang, Yida Wang, Yuanzhong Xu, Danyang Zhuo, Eric P. Xing, Joseph E. Gonzalez, and Ion Stoica. Alpa: Automating inter- and Intra-Operator parallelism for distributed deep learning. In *USENIX OSDI*, 2022.

[41] Sizhe Zheng, Jin Fang, Xuegui Zheng, Qi Hou, Wenlei Bao, Ningxin Zheng, Ziheng Jiang, Dongyang Wang, Jianxi Ye, Haibin Lin, Li-Wen Chang, and Xin Liu. Tilelink: Generating efficient compute-communication overlapping kernels using tile-centric primitives. In *MLSys*, 2026.

[42] Kan Zhu, Yufei Gao, Yilong Zhao, Liangyu Zhao, Gefei Zuo, Yile Gu, Dedong Xie, Tian Tang, Qinyu Xu, Zihao Ye, Keisuke Kamahori, Chien-Yu Lin, Ziren Wang, Stephanie Wang, Arvind Krishnamurthy, and Baris Kasikci. NanoFlow: Towards optimal large language model serving throughput. In *OSDI*, 2025.

A Energy Efficiency of Constant Frequency

Below, we restate Theorem 1 in more mathematical terms.

Theorem 1 (Energy Efficiency of Constant Frequency). *Let $f(t)$ denote the GPU frequency over a time interval $[0, T]$, and let $\bar{f} = \frac{1}{T} \int_0^T f(t) dt$ be its time-average. Under the following assumptions:*

1. *Dynamic power scales cubically with frequency: $P_{\text{dyn}}(t) = k \cdot f(t)^3$ for some constant $k > 0$.*
2. *Static power is constant: $P_{\text{static}}(t) = P_s$ for some constant $P_s \geq 0$.*
3. *Execution time depends only on average frequency: workloads with the same average frequency \bar{f} complete in the same time T . This is supported by empirical observations from Kareus optimization results.*

Then the total energy consumption is minimized when frequency is held constant at \bar{f} .

Proof. Total energy is the sum of dynamic and static energy:

$$E_{\text{total}} = E_{\text{dyn}} + E_{\text{static}} = \int_0^T k \cdot f(t)^3 dt + P_s \cdot T.$$

By Assumption 3, T is identical for both the fluctuating and constant frequency cases. Thus, static energy $E_{\text{static}} = P_s \cdot T$ is equal in both cases.

For dynamic energy, consider the function $g(x) = x^3$, which is convex for $x > 0$ since $g''(x) = 6x > 0$. By Jensen’s Inequality:

$$g(\bar{f}) = \bar{f}^3 \leq \frac{1}{T} \int_0^T f(t)^3 dt.$$

Multiplying both sides by kT :

$$E_{\text{dyn}}^{\text{constant}} = kT \cdot \bar{f}^3 \leq k \int_0^T f(t)^3 dt = E_{\text{dyn}}^{\text{fluctuating}}.$$

Equality holds if and only if $f(t) = \bar{f}$ almost everywhere, i.e., when frequency is constant. Therefore:

$$E_{\text{total}}^{\text{constant}} \leq E_{\text{total}}^{\text{fluctuating}},$$

with strict inequality when $f(t)$ varies over time. \square

Implications for GPU frequency scaling. This theorem explains why frequency fluctuation due to power limits can be energy-inefficient. When a GPU operates at a high frequency and triggers power throttling, the instantaneous frequency fluctuates, while the time-averaged frequency remains close to what could be achieved by operating steadily at a lower frequency. Consequently, the execution time—and thus static energy consumption—are the same as those under steady lower-frequency operation. However, this fluctuation incurs higher dynamic energy consumption because dynamic power is a strictly convex function of frequency. By Jensen’s Inequality, any variance in frequency increases the expected dynamic energy consumption.

B Global Solution Space

The global solution space of combining GPU frequency, SM allocation, and kernel launch timing is extremely large. In this section, we illustrate the space using the NVIDIA A100 GPU as an example.

GPU frequencies. Supported GPU frequencies by A100 are from 210 MHz to 1,410 MHz at a stride of 15 MHz. We restrict the search space to 900 MHz–1,410 MHz (35 choices) because lowering the frequency below 900 MHz no longer reduces energy.⁹

SM allocations. A100 has 108 SMs, and we restrict the search space to up to 30 SMs because allocating additional SMs beyond this empirically no longer improved communication latency. This leaves 30 choices for SM allocation.

Kernel launch timing. Finally, given a sequence of computation and communication kernels, possible execution orders can be expressed as a recurrence relation, which enumerates the number of subproblems. We elaborate on this formulation in the following paragraphs. In summary, for a typical LLM composed of Transformer blocks, this can result in 81 possible groupings, leading to a *global solution space* with in total 85,050 candidates.

Formulation of launch timing. Kareus generalizes the nanobatching scheme to eliminate dependencies between computation and communication, which enables overlap and results in two operation sequences:

$$\mathcal{S}_1 = \{O_0, O_1, \dots, O_i\}, \quad \mathcal{S}_2 = \{O'_0, O'_1, \dots, O'_j\}.$$

where operations within the same sequence must be executed in order, while operations across sequences are independent and may overlap. We regard the consecutive communication operations as a single operation. The time–energy frontier of the launch timing schedule can be formulated as a dynamic programming (DP) recurrence:

$$\mathcal{P}(i, j) = \min_{\text{Pareto}} \begin{cases} (E(O_i) + E(\mathcal{P}(i+1, j)), T(O_i) + T(\mathcal{P}(i+1, j))) \\ (E(O'_j) + E(\mathcal{P}(i, j+1)), T(O'_j) + T(\mathcal{P}(i, j+1))) \\ (E(O_i \parallel O'_{j..j+k}), T(O_i \parallel O'_{j..j+k})) + \mathcal{P}(i+1, j+k) \\ (E(O'_j \parallel O_{i..i+k}), T(O'_j \parallel O_{i..i+k})) + \mathcal{P}(i+k, j+1) \end{cases}$$

Here, $O_i \parallel O'_{j..j+k}$ means overlapping operation O_i with a subsequence $\{O'_j, \dots, O'_{j+k}\}$; the notation is symmetric for the opposite case, $O'_j \parallel O_{i..i+k}$. The cost functions $E(\cdot)$ and $T(\cdot)$ account for the interference when overlapping.

This recurrence enumerates the time and energy of all single operations and all feasible overlap patterns between the

⁹Power reduction slows down but time increases, leading to higher energy.

two sequences. For a typical Transformer block with 9 computation operations and 1 AllReduce, if we restrict overlap to occur only between communication and computation and cap the maximum overlap length at 9 (assuming the communication is no longer than a full Transformer block), there are 81 possible overlap patterns. Including the non-overlapped cases, this yields a total of 91 subproblems.

C Adaptation of MBO Hyperparameters

In this section, we describe how Kareus configures MBO hyperparameters. Some are adapted across different partitions based on partition complexity, while others remain fixed.

Search space. For GPU frequency, we restrict the search space to 900–1,410 MHz with a stride of 30 MHz, since the time and energy differences between adjacent 15 MHz settings are marginal. For SM allocation, the search space is determined by the communication group size. If the number of GPUs in a communication group is fewer than 4, we search SM allocations from 1 to 20 with a stride of 1. If the group size is 4 or larger (e.g., the common cases of 4 and 8), we search SM allocations from 3 to 30 with a stride of 3. For launch timing, we enumerate all computation operators within a partition and exclude options that always lead to exposed communication, such as launching AllReduce from Linear2 in Figure 3a.

Sample size. Our goal is to control the total profiling time while preserving the quality of the time–energy frontier. We adopt a relatively large initialization set for informative exploration and scale the batch search budget based on partition complexity. Specifically, we classify partitions into three categories: *small* partitions containing only one computation, *medium* partitions containing 2–3 computations, and *large* partitions containing more than three computations. We then configure the sample sizes as follows: initial sample size $N_{\text{init}} = 36$, maximum number of batches $B_{\text{max}} = 3$, batch size $k = 16$ for small partition; $N_{\text{init}} = 48$, $B_{\text{max}} = 4$, $k = 16$ for medium partition; $N_{\text{init}} = 96$, $B_{\text{max}} = 4$, $k = 32$ for large partition. We set the proportions of the total energy pass, dynamic energy pass, static energy pass, and uncertainty pass to 0.4, 0.2, 0.2, and 0.2, respectively. As shown in Section 6.4, the MBO overhead of Kareus is controlled within two hours on average.

XGBoost hyperparameters. Since the configuration space is three-dimensional, we adopt XGBoost hyperparameter settings commonly used for low-dimensional regression. To ensure fast and stable convergence while avoiding overfitting, we use relatively shallow trees with $\text{max_depth} = 6$, a high learning rate $\eta = 0.3$, and a modest model capacity with $\text{num_boost_round} = 100$. For the bootstrap ensemble, we set the ensemble size to 5, use a bootstrap sampling fraction of 0.8, and vary the random seed across bootstrap resamples.

HV reference point. At each batch iteration, we compute the HV reference point using values slightly worse than the

worst observed measurements to ensure boundedness. Specifically, we set $r = (1.1 \times \max T(x), 1.1 \times \max E(x))$.

Stopping conditions. The MBO algorithm is terminated when either a sufficient number of samples has been collected or the objective has converged, according to the following criteria: (1) Stop after a fixed number of batches B_{max} . (2) After each batch, compute the dominated hypervolume of the measured frontier. Stop if the moving average of the relative HV improvement over the last R batches falls below ϵ .

We set the window size in the stopping criterion to $R = 2$ and the convergence threshold to $\epsilon = 10^{-3}$. Energy and time are normalized throughout the MBO process, ensuring stable stopping behavior across partitions.

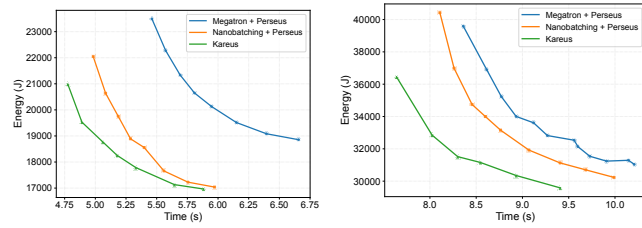
D Time–Energy Frontier

D.1 End-to-end Results

Figure 11 shows the time–energy frontiers measured on the testbed GPUs for all model configurations.

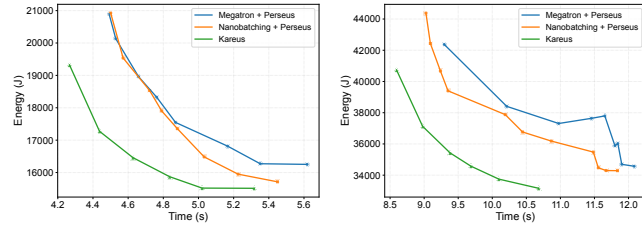
D.2 Large-scale Emulation

Figure 12 shows the time–energy frontiers in large-scale emulation for Llama 3.3 70B across different numbers of micro-batches.



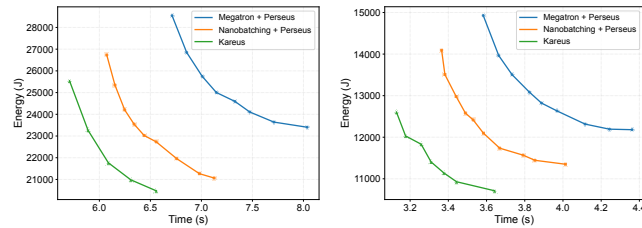
(a) *Llama 3.2 3B, CP=1, TP=8, $\mu\text{BS}=8$, Seq=4096*

(b) *Llama 3.2 3B, CP=2, TP=4, $\mu\text{BS}=16$, Seq=4096*



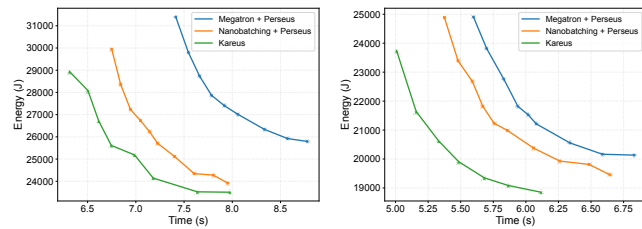
(c) *Llama 3.2 3B, CP=2, TP=4, $\mu\text{BS}=8$, Seq=4096*

(d) *Llama 3.2 3B, CP=2, TP=4, $\mu\text{BS}=8$, Seq=8192*



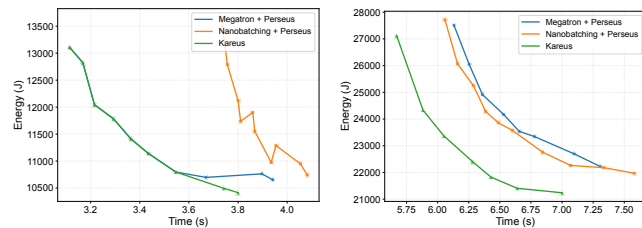
(e) *Qwen 3 1.7B, CP=1, TP=8, $\mu\text{BS}=16$, Seq=4096*

(f) *Qwen 3 1.7B, CP=1, TP=8, $\mu\text{BS}=8$, Seq=4096*



(g) *Qwen 3 1.7B, CP=1, TP=8, $\mu\text{BS}=8$, Seq=8192*

(h) *Qwen 3 1.7B, CP=2, TP=4, $\mu\text{BS}=16$, Seq=4096*



(i) *Qwen 3 1.7B, CP=2, TP=4, $\mu\text{BS}=8$, Seq=4096*

(j) *Qwen 3 1.7B, CP=2, TP=4, $\mu\text{BS}=8$, Seq=8192*

Figure 11: [Experiments] Time-energy frontiers of Megatron-LM + Perseus, Nanobatching + Perseus, and Kareus for all model configurations. CP: Context Parallelism, TP: Tensor Parallelism, μBS : Microbatch Size, Seq: Sequence Length.

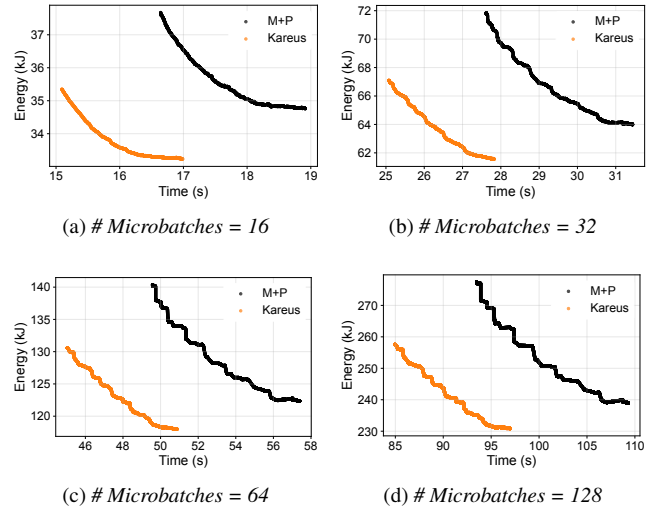


Figure 12: [Emulation] Iteration time-energy frontiers of Megatron-LM + Perseus and Kareus for Llama 3.3 70Bs.